Nanoscale

Accepted Manuscript

This article can be cited before page numbers have been issued, to do this please use: J. Li, Y. cheng, W. Wang and X. Yan, *Nanoscale*, 2018, DOI: 10.1039/C8NR04414G.

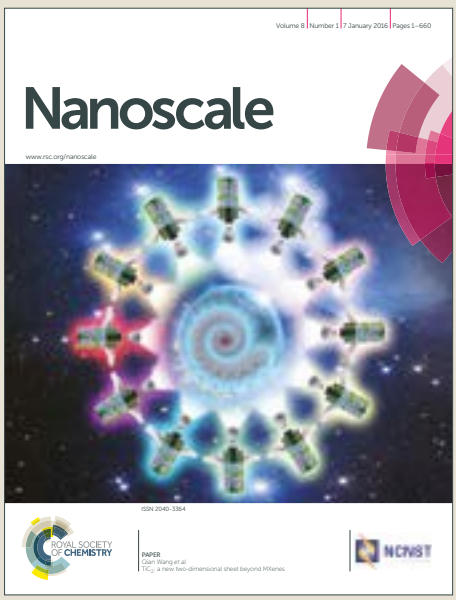

ROYAL SOCIETY OF CHEMISTRY

rsc.li/nanoscale

View Article Online
DOI: 10.1039/C8NR04414G

Nanoscale

ARTICLE

Functionalized gold and persistent luminescence nanoparticles based ratiometric absorption and TR-FRET nanoplatform for high-throughput sequential detection of L-cysteine and insulin

Received 00th January 20xx,
Accepted 00th January 20xx

DOI: 10.1039/x0xx00000x

www.rsc.org/

Juan Li[a,b,c], Cheng Yang[c], Wen-Long Wang[c], Xiu-Ping Yan*[,a,b,c]

In vitro diagnostic is a crucial component of healthcare systems for early diagnosis of diseases and follow-up therapy, generally makes clinical diagnosis faster, easier, and painless to patients. Herein, we report a dual-signaling nanoplatform for ratiometric absorption and time resolved fluorescence resonance energy transfer based on L-cysteine mediated agminated gold nanoparticles and long afterglow nature of persistent luminescence nanoparticles. With this nanoplatform, we achieved high-throughput sequential detection of L-cysteine and Insulin in human serum without matrix interference. The proposed nanoplatform showed excellent linearity and precision for the determination of L-cysteine in the range of 10 nM to 5.5 μM with the limit of detection (LOD) of 2.2 nM, and for the detection of insulin in the range of 12 pM to 3.44 nM with the LOD of 2.06 pM. The developed dual-signaling nanplatform was successfully applied for sequential determination of L-cysteine and insulin in human serum.

1. Introduction

In vitro diagnostic (IVD) is indispensable for routine patient management.[1] It allows early-stage intervention and post-medical care expenditure reduction.[2] Most of the analytes for IVD derive from body specimens, including blood, urine, saliva and tissue biopsies, and enable rapid and real-time treatment decision.[3]

Abnormal levels of L-cysteine (L-Cys) and insulin (Ins) in human serum are associated with diabetes and related diseases. L-Cys is essential for maintaining intracellular thiol redox potential. It is imperative for detoxification and metabolism of biological system, and capable of indicating some diseases.[4,5] For instance, a number of relevant disorders and diseases are associated with the deficiency of L-Cys, including skin lesions, edema, slow growth, somnolence, osteoporosis, cervical dysplasia and Alzheimer's disease.[6,7] Moreover, diabetic patients have low blood levels of L-Cys.[8] Ins regulates the physiological metabolism of carbohydrates and fats.[8] Diabetes and obesity result from Ins related metabolic disorders.[9-11] In addition, Ins is utilized for cheating in athletic competition.[12] Numerous epidemiological and preclinical studies show that Ins is a potential biomarker of breast cancer.[13]

For the above reasons, an easy-to-control method for highly sensitive and selective detection of L-Cys and Ins in biological fluids is of significance in IVD. There are several methods for the determination of L-Cys or Ins, such as immunologic technique,[14] surface plasmon resonance technique,[15] Raman spectroscopy,[16] chemiluminescence,[17] and electrochemical technique.[18] These methods are cost-effective and highly sensitive, but mainly focus on the detection of single target. Besides, these methods suffer from time-consuming and complicated operation procedures, or the need for special chip and large volume of sample. Currently, ratiometric probes and aptamer-mediated nanosensors attract much attention for biochemical analysis and clinical diagnosis due to their simplicity, rapidity, excellent sensitivity, good specificity, low cost and ease of operation.[19-21]

Herein, we report a ratiometric absorption (Ratio-Abs) and time-resolved fluorescence resonance energy transfer (TR-FRET) nanoplatform for high-throughput sequential detection of L-Cys and Ins based on functionalized persistent luminescence nanoparticles (PLNPs) and gold nanoparticles (AuNPs). The application of Ratio-Abs and TR-FRET effectively eliminates the interference from matrix and autofluorescence, while the use of multi-mode microplate reader allows high-throughput detection.

2. Experimental section

2.1 Materials

[a] State Key Laboratory of Food Science and Technology, Jiangnan University, Wuxi 214122, China
[b] International Joint Laboratory on Food Safety, Jiangnan University, Wuxi 214122, China
[c] Institute of Analytical Food Safety, School of Food Science and Technology, Jiangnan University, Wuxi 214122, China
E-mail: xpyan@jiangnan.edu.cn

Electronic Supplementary Information (ESI) available: Insulin binding aptamer and it's complementary sequence, Figures S1-S18, and Tables S1-S2. See DOI: 10.1039/x0xx00000x

All reagents are at least analytical grade unless specified and used as received without purification. Sodium citrate, tetrachloroauric acid ($HAuCl_4$), L-Cys, $Ga(NO_3)_3$, $Zn(NO_3)_2$ $6H_2O$, $Cr(NO_3)_3$ $9H_2O$, aminopropyltriethoxysilane (APTES), hydroxyl functionalized polyethylene glycol carboxylic acid (OH-PEG12-COOH), N-(3-dimethylaminopropyl)-N'-ethylcarbodiimide hydrochloride (EDC), human immunoglobulin G (IgG), human serum albumin (HSA), glucose (Glu), glutathione (GSH) and L-homocysteine (Hcy) were purchased from Sigma–Aldrich (St. Louis, MO, USA). Sodium dodecyl sulfate (SDS) and N-hydroxysuccinimide (NHS) were purchased from Aladdin (Shanghai, China). Carboxylated insulin binding aptamer (COOH-IBA), and thiol-functionalized partial complementary sequence (SH-CS) of IBA were manufactured by Shanghai Sangon Biological Engineering Technology & Services Co. (Shanghai, China). Ins, and amino acids were bought from National Institutes for Food and Drug Control (Beijing, China). Ethanol, ammonium hydroxide, hydrochloride acid, and concentrated nitric acid and 2-mercaptoethanol (ME) were purchased from Sinopharm Chemical Reagent (Beijing, China). Human serum samples were collected from healthy persons with informed consent. Ultrapure water was obtained from Wahaha group co. (Hangzhou, China).

2.2 Synthesis of AuNPs and PLNPs

The AuNPs were prepared according to classic sodium citrate synthesis method.[22] Briefly, $HAuCl_4$ (100 mL, 0.1 g L^{-1}) was boiled for 10 min, 2.6 mL sodium citrate (1% w/v) was then injected with high-speed stirring. After stirring and boiling for another 10 min, the solution turned reddish-orange. The resulting colloidal gold solution was cooled to ambient temperature. The prepared citrate-capped AuNPs was stored at 4 ^{o}C for further use.

The PLNPs were synthesized via a hydrothermal process.[23] Briefly, aqueous solutions of $Ga(NO_3)_3$ (1 mL, 2 M), $Zn(NO_3)_2$ (2 mL, 1 M) and $Cr(NO_3)_3$ (4 mL, 1 mM) were mixed in a Teflon-lined autoclave. The mixture was made up to 30 mL with ultrapure water, adjusted to pH 9, and kept stirring at room temperature for 3 h. Then, the Teflon-lined autoclave was sealed, heated at 220 ^{o}C for 12-h hydrothermal reaction, and naturally cooled to room temperature. The resulting PLNPs were collected via centrifugation, washed with 0.01 M HCl and isopropanol, and dried in a vacuum oven for further use.

2.3 Functionalization of AuNPs and PLNPs

For the preparation of complementary sequence modified gold nanoparticles (AuNP-CS), SH-CS (560 μL, 0.5 μM), AuNPs (6 mL, 16.7 nM) and SDS (78 μL, 10% w/v) were mixed in phosphate buffer (10 mM, pH 7.4). NaCl solution (360 μL, 0.2 M) was slowly added to the mixture every one hour during 20-h

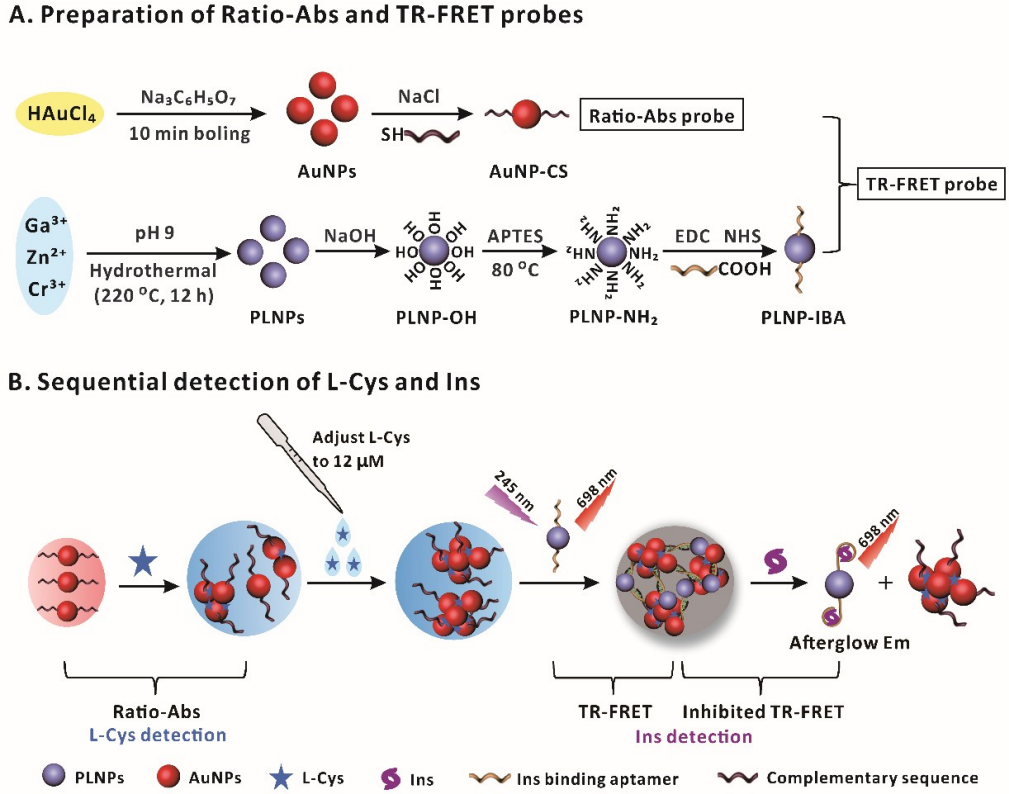

Fig. 1 Schematic diagram of Ratio-Abs and TR-FRET dual-signaling nanoplatform for sequential detection of L-Cys and Ins. IBA represents Ins binding aptamer, complementary sequence represents the partial complementary sequence of IBA. Em is short for emission.

View Article Online
DOI: 10.1039/C8NR04414G

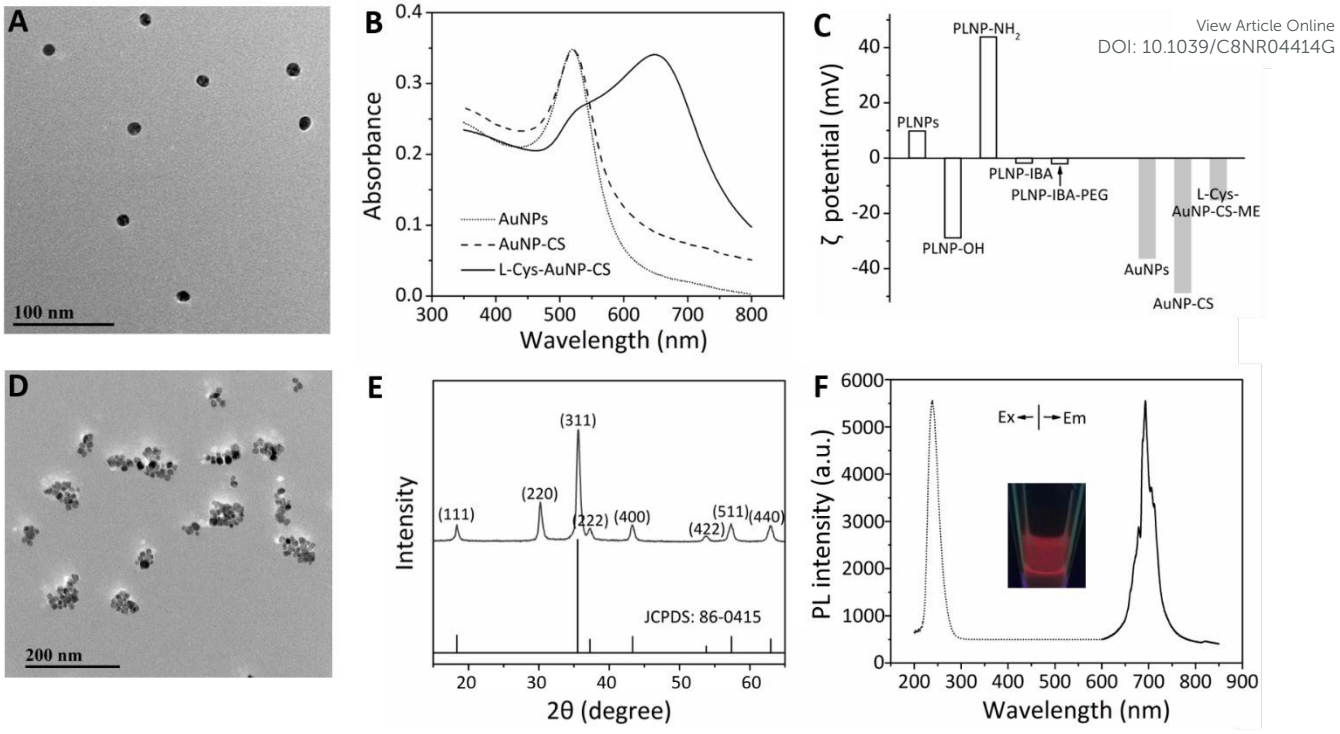

Fig. 2 (A) TEM image of the AuNPs. (B) Absorption spectra of AuNPs, AuNP-CS and L-Cys-AuNP-CS (L-Cys mediated aggregated AuNP-CS). (C) ζ potentials of bare and functionalized nanoparticles. L-Cys-AuNP-CS-ME represents ME blocked L-Cys-AuNP-CS. (D) TEM image of PLNPs. (E) XRD pattern of the PLNPs. (F) Excitation (Ex) and emission (Em) spectra of the PLNPs, and the photograph of 254 nm UV lamp excited PLNPs.

reaction. The mixture was centrifuged at 13000 rpm for 20 min, and the precipitate was washed with Tris–HCl buffer (10 mM, pH 7.2) to obtain AuNP-CS.

Amino functionalized PLNPs (PLNP-NH_2) were prepared according to our previous report.[24] PLNP-NH_2 (5 mg), COOH-IBA (4 nmol), NHS (8 nmol) and EDC (16 nmol) were mixed in PBS (11 mL, 0.01M, pH 7.4) and incubated at room temperature for 30 min with shaking in dark. OH-PEG12-COOH (4 μmol), NHS (8 μmol) and EDC (16 μmol) were added for another 2-h reaction. The prepared IBA modified PLNPs (PLNP-IBA) blocked with PEG (PLNP-IBA-PEG) were collected via centrifugation and washed twice with Tris–HCl (10 mM, pH 7.2).

2.4 Instrumentation

Transmission electron microscopy (TEM) images were recorded on a JEM-2100 transmission electron microscope at an acceleration voltage of 200 kV (JEOL, Japan). X-ray diffraction (XRD) analysis was performed on a D2 PHASER powder diffractometer with a radiation source of CuKα (Bruker, Germany). The hydrodynamic diameter and ζ potential were measured on a Nano ZS Zetasizer with 633 nm He–Ne laser (Malvern, UK). UV–vis absorption spectra were obtained on a UV-3600PLUS UV–vis–NIR spectrophotometer (Shimadzu, Japan). The phosphorescence spectra were obtained on an F-7000 fluorescence spectrophotometer (Hitachi, Japan). The persistent luminescence (PL) decay curves were recorded on a JY FL-3 hybrid steady-state and lifetime spectrofluorometer (Horiba, Japan). Fourier transform infrared spectra (FTIR) were acquired on an IS10 FTIR spectrometer (Nicolet, USA). Sequential detection of L-Cys and Ins was performed on Cytation 3 multi-mode microplate reader (BioTek, USA).

2.5 Sequential detection of L-Cys and Ins

Human serum samples were subjected to a 100-fold dilution before analysis. Standard solution containing certain amount of L-Cys and Ins or sample solution (25 μL) were thoroughly mixed with AuNP-CS (25 μL, 33.4 nM) in the 96-well plate for 5 min incubation. Then, the plate was loaded onto the multi-mode microplate reader to obtain the absorbance at 520 nm and 660 nm (A_{520} and A_{660}) for the determination of L-Cys. Thereafter, the concentration of L-Cys in the mixture in each well was adjusted to 12 μM by adding the solution of L-Cys. After adding ME (5 μL, 10 μM), the mixture was diluted to volume with ultrapure water for 3-min incubation. PLNP-IBA (50 μL, 50 μg mL^{-1}) was added to each well for 15 min specific recognition and PL intensity at 698 nm (with excitation at 245 nm and delay time of 100 microseconds) was recorded for the determination of Ins.

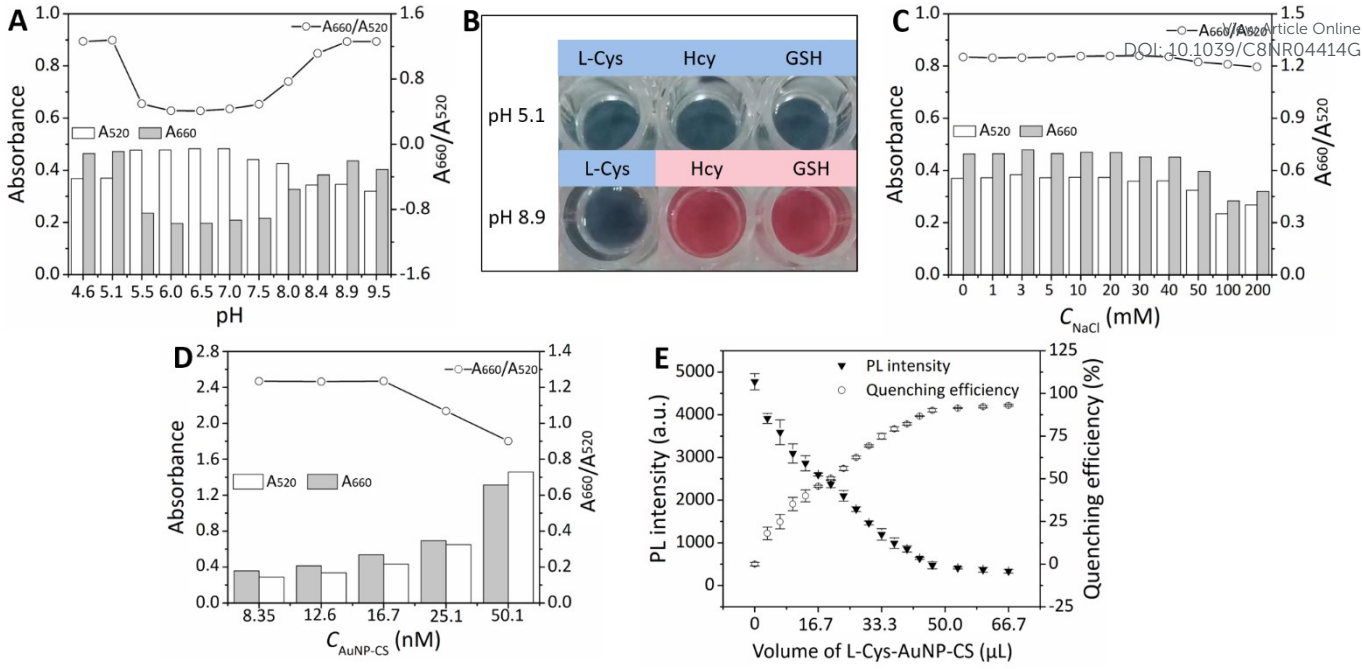

Fig. 3 (A) (B) Effect of pH on L-Cys mediated AuNP-CS aggregation. (C) Effect of NaCl concentration on L-Cys mediated AuNP-CS aggregation. (D) Effect of the concentration of AuNP-CS. (E) Effect of the volume of L-Cys-AuNP-CS (16.7 nM) on the PL quenching of PLNP-IBA (50 μL, 50 μg mL^{-1}).

3. Results and discussion

3.1 Design of Ratio-Abs and TR-FRET dual-signaling nanoplatform for sequential detection of L-Cys and Ins

Fig. 1 shows the design of a dual-signaling nanoplatform of Ratio-Abs and TR-FRET for sequential detection of L-Cys and Ins. Owing to the high molar extinction coefficient and tunable absorption of AuNPs, and the long afterglow nature of PLNPs, AuNPs and PLNPs were prepared as signal elements. The presence of L-Cys enables significant red shift of the absorption peak of AuNP-CS due to L-Cys mediated aggregation of AuNP-CS, providing a Ratio-Abs signal for the detection of L-Cys.

We then employed PLNP-IBA and aggregated AuNP-CS as the donor and the acceptor, respectively, to design a TR-FRET system. The overlap between the emission spectrum of PLNPs and the absorption spectrum of the aggregated AuNPs as well as the complementary ssDNA interaction between IBA and CS ensures the effective occurrence of TR-FRET between PLNP-IBA and aggregated AuNP-CS, leading to PL quenching of the PLNPs. However, the presence of Ins inhibits the TR-FRET and turns on the PL of the PLNPs due to strong interaction between Ins and IBA. Thus, we can realize sequential detection of L-Cys and Ins based on this dual-signaling nanoplatform by taking full advantage of the inherent optical properties of AuNPs and PLNPs.

3.2 Preparation and characterization of the dual-signaling probe

To fabricate the dual-signaling nanoplatform, AuNPs and PLNPs were prepared as signal elements. The bare AuNPs showed a uniform size of 12 nm (calculated from 100 randomly selected particles) (Fig. 2A) and a characteristic absorption peak at 520 nm (Fig. 2B). SH-CS modification of the AuNPs through Au−S covalent bonds led to no significant change in absorption peak (Fig. 2B) and particle size, but an increase in hydrodynamic diameter from 13.3 ± 2.1 nm to 18.5 ± 2.6 nm (Fig. S1 and S2 †). CS coating made the AuNPs more negatively charged, whereas further ME blocking had the AuNPs less negatively charged (Fig. 2C). Moreover, the prepared AuNP-CS possess good stability from pH 5 to 10 (Fig. S3†).

The as-prepared PLNPs ($ZnGa_2O_4:Cr^{3+}$) gave a particle size of 9 ± 2 nm (calculated from 100 randomly selected particles) (Fig. 2D and Fig. S4†) with a pure spinel phase structure of zinc gallate (Fig. 2E). The PLNPs can be excited with UV light from 220 nm to 280 nm to give a NIR emission band at 698 nm due to the ^2E - $^4A_2$ transition of the distorted Cr^{3+} ions in the zinc gallate host (Fig. 2F). The PLNPs in aqueous solution (0.8 mg mL^{-1}) exhibited similar optical properties during seven cycles with reactivation with a Xe lamp at 254 nm (Fig. S5†), indicate excellent PL stability of the prepared PLNPs.

Surface modifications of PLNPs were confirmed by FTIR, ninhydrin test, and ζ potential. The strong absorption bands of O−Si−O stretching vibration at 1115 and 1022 cm^{-1}, asymmetric and symmetric -CH_2- stretching bands at 2931 and 2858 cm^{-1}, and N−H stretching bands between 3416 and 3243 cm^{-1} in the FTIR spectra of PLNP-NH_2 (Fig. S6†) indicate the successful condensation reaction of APTES on the surface of PLNPs. Ninhydrin test shows a strong absorption at 570 nm

(Fig. S7†), further confirming the successfully amination of PLNPs. Hydroxylation and amination made the ζ potential of PLNPs change from +9.78 to −28.9 mV and +43.8 mV, respectively, whereas further modification with COOH-IBA and OH-PEG-COOH had PLNPs slight negatively charged (Fig. 2C). Plenty of OH-PEG-COOH blocked on the surface of PLNP-IBA could prevent the nonspecific adsorption. In addition, the prepared PLNP-IBA gave similar luminescent properties in a pH range of 5-10 (Fig. S8†).

3.3 Factors affecting L-Cys mediated aggregation of AuNP-CS

The presence of L-Cys in AuNP-CS solution resulted in a significant red shift of absorption peak from 520 nm to 660 nm (Fig. 2B), and obvious increase of hydrodynamic diameter from 18.5 ± 2.6 nm to 86 ± 3.0 nm (Fig. S3 and S9†), confirming L-Cys mediated aggregation of AuNP-CS (Fig. S10†). The time dependence of the absorbance of the two peaks at 520 nm and 660 nm along with the ratio of A_{660} to A_{520} (A_{660}/A_{520}) is shown in Fig. S11†. The absorbance of the peak at 520 nm decreased while that at 660 nm and A_{660}/A_{520} increased significantly within 2 min in the presence of L-Cys (12 μM), then reached plateau within 5 min.

pH plays an important role in L-Cys mediated aggregation of AuNP-CS (Fig. 3A and 3B). L-Cys significantly prompted AuNP-CS agglomeration at pH<5.1 or >8.9 in accompany with color change from red to purple or blue due to intermolecular electrostatic interaction and van der Waals force.[25] Hcy and GSH also led to the agglomeration of AuNPs at pH 5.1, but no agglomeration at pH 8.9 (Fig. 3B) within 5 min due to the easiness for the formation of their five-membered ring transition states through intramolecular hydrogen abstraction at higher pH,[26] providing a possibility for selective detection of L-Cys in the presence of Hcy and GSH.

NaCl had no influence on AuNP-CS aggregation in the studied concentration range of 0-200 mM (Fig. 3C). The extent of the aggregation of AuNP-CS highly depended on its concentration. The ratio of A_{660}/A_{520} in the presence of 12 μM L-Cys increased as the concentration of AuNP-CS decreased, then reached maximum at 16.7 nM AuNP-CS (Fig. 3D and Fig. S12†).

3.4 Factors affecting TR-FRET

To achieve high energy transfer efficiency, we optimized the amount of the acceptor (L-Cys-AuNP-CS) for quenching a certain amount of donor (PLNP-IBA, 50 μL, 50 μg mL^{-1}). Before optimization, we adjusted the concentration of L-Cys to 12 μM in AuNP-CS to ensure the reliability for quantitative determination and blocked the L-Cys-AuNP-CS with sufficient ME to reduce nonspecific adsorption. The result indicates that 50 μL of L-Cys-AuNP-CS (16.7 nM) could quench the PL of PLNP-IBA almost completely (Fig. 3E).

Kinetic study demonstrates that the TR-FRET signal (PL intensity) rapidly increased in the first 5 min, then became stable after 12 min in the presence of Ins (1.5 nM). Therefore, 15 min was selected to collect the PL intensity for subsequent detection (Fig. S13†).

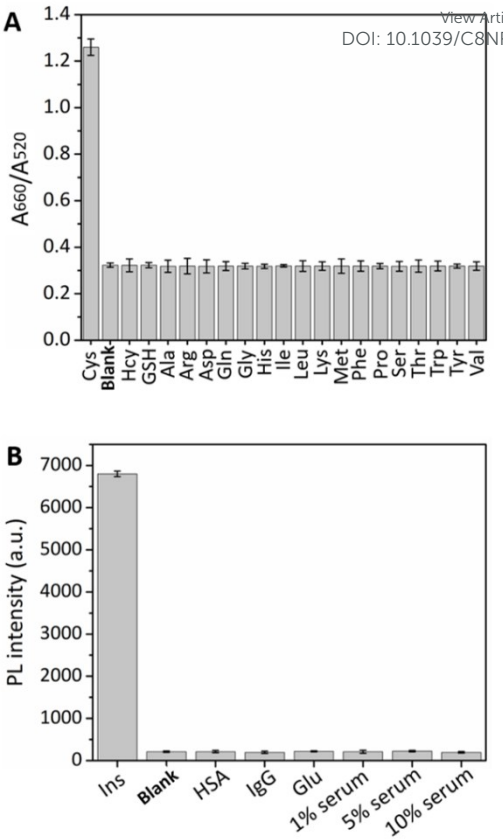

Fig. 4 (A) Selectivity for the detection of L-Cys (6 μM for all the species tested). (B) Selectivity for the detection of Ins (2.0 nM for Ins; 50 nM for HSA, IgG, and Glu).

3.5 Selectivity of the developed dual-signaling nanoplatform

To test the selectivity of the proposed assay for the detection of L-Cys, the same concentration (6 μM) of L-Hcy, GSH and 18 amino acids (including alanine (Ala), arginine (Arg), aspartic acid (Asp), L-cysteine (L-Cys), glutamic acid (Gln), glycince (Gly), histidine (His), isoleucine (Ile), leucine (Leu), lysine (Lys), methionine (Met), phenylalanine (Phe), proline (Pro), serine (Ser), threonine (Thr), tryptophan (Trp), tyrosine (Tyr) and valine (Val)) were detected with Ratio-Abs. Tris-HCl buffer solution (blank) was used as a control. The results show that only L-Cys gave significant value of A_{660}/A_{520} whereas L-Hcy, GSH and other 17 amino acids showed negligible difference of A_{660}/A_{520} in comparison with the blank (Fig. 4A and Fig. S14†).

We also investigated the selectivity of the developed assay for the detection of Ins by determining other interferents, human immunoglobulin G (IgG) (50 nM), human serum albumin (HSA) (50 nM), glucose (Glu) (50 nM), and serum (1%, 5%, and 10%). The results show that only Ins (2.0 nM) produced a significant signal while the interferents did not result in distinguishable signals from the blank control (Fig. 4B and Fig. S15†). The high selectivity of this assay benefits from the high affinity between Ins and IBA. The above results reveal the good selectivity of the developed dual-signaling nanoplatform for the detection of L-Cys and Ins.

View Article Online
DOI: 10.1039/C8NR04414G

Table 1 Analytical characteristic data of the Ratio-Abs and TR-FRET nanoplatform

Target	Calibration function[a]	Determination coefficient (R^2)	Liner range	LOD	RSD (%) (n=11)
L-Cys	$A_{660}/A_{520} = 0.1534\ C_{L\text{-}Cys} + 0.437$	0.9973	10 nM – 5.5 μM	2.2 nM	2.4
Ins	$I = 2120.2\ \lg C_{Ins} + 4295.7$	0.9906	12 pM – 3.44 nM	2.06 pM	2.1

[a] I represents PL intensity.

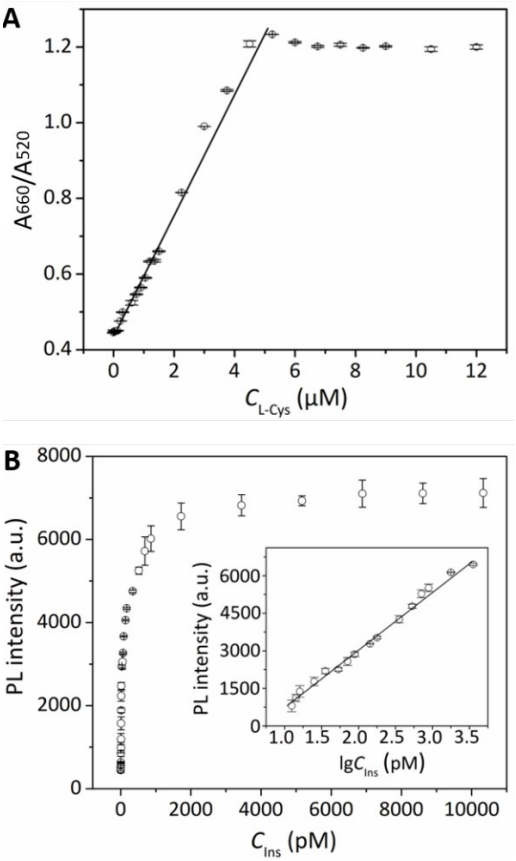

Fig. 5 (A) Plot of A_{660}/A_{520} against L-Cys concentration. (B) Plot of PL intensity against Ins concentration, inset shows the liner calibration curve of PL intensity against the logarithm of Ins concentration.

3.6 Analytical performance of the developed dual-signaling nanoplatform

The analytical characteristic data of the Ratio-Abs and TR-FRET nanoplatform are summarised in Table 1. The Ratio-Abs signal depends on the aggregation degree of AuNP-CS caused by L-Cys at various concentrations (Fig. 5A and Fig. S16†). The A_{660}/A_{520} increases linearly with the concentration of L-Cys in the range of 10 nM to 5.5 μM with a determination coefficient of 0.9973 and a linear regression equation $A_{660}/A_{520} = 0.1534C_{L\text{-}Cys} + 0.437$. In addition, the PL intensity (I) increases with the logarithm of Ins concentration with a linear regression equation $I = 2120.2\ \lg C_{Ins} + 4295.7$ in a wide range from 12 pM to 3.44 nM with a determination coefficient of 0.9906 (Fig. 5B and Fig. S17†). The limits of detection (LOD) (3s) of L-Cys and Ins are 2.2 nM and 2.06 pM, respectively, which are comparable with some reported methods for L-Cys and Ins detection separately (Table S1† and S2†). The precisions for 11 replicate detections of L-Cys at 1.0 μM and Ins at 0.25 nM are 2.4% and 2.1% (relative standard deviation, RSD), respectively. Our method allows high-throughput detection of hundreds of samples within half an hour using 96-well plates.

3.7 Application to real sample analysis

The long-lasting afterglow nature of PLNPs allows detection without interference from autofluorescence and scattering light from biological matrixes encountered under in situ excitation (Fig S18†). The proposed method was applied to the determination of L-Cys and Ins in human serum (Table 2). The L-Cys and Ins in six human serum samples were determined to be 4.01-4.21 μM and 114-160 pM, respectively. Quantitative recoveries were obtained for L-Cys (1 μM) and Ins (172 pM) spiked in the human serum samples. The inhibited TR-FRET was successfully employed to detect Ins in human serum samples without fluorescent background noise. The above results demonstrate the potential applicability of the developed nanoplatform for sequential detection of L-Cys and Ins in clinical samples.

4. Conclusions

In summary, we have developed a Ratio-Abs and TR-FRET dual-signaling nanoplatform for sequential determination of L-Cys and Ins in human serum. The present dual-functional nanoplatform not only effectively eliminates the interference from biological matrix, but also opens a new perspective for developing sensitive, selective, high-throughput, low-consumption and multi-detection in early-stage disease screening, follow-up care, food safety inspection and environment monitoring.

Table 2 Analytical results for sequential determination of L-Cys and Ins in serum

View Article Online
DOI: 10.1039/C8NR04414G

Sample	Analyte spiked		Concentration found (Mean ±*s*, n=9)		Recovery (%) (Mean ±*s*, n=9)	
	L-Cys (μM)	Ins (pM)	L-Cys (μM)	Ins (pM)	L-Cys	Ins
Serum 1	0	0	4.08 ±0.09	156 ±3		
	1.00	172	5.06 ±0.01	331 ±5	98.0 ±0.2	102.0 ±1.5
Serum 2	0	0	4.13 ±0.03	114 ±2		
	1.00	172	5.16 ±0.09	277 ±9	103.0 ±1.7	94.8 ±3.2
Serum 3	0	0	4.02 ±0.03	158 ±3		
	1.00	172	5.08 ±0.19	343 ±11	107.0 ±3.7	107.5 ±3.2
Serum 4	0	0	4.21 ±0.05	122 ±5		
	1.00	172	5.14 ±0.11	308 ±7	93.0 ±2.1	108.1 ±2.3
Serum 5	0	0	4.01 ±0.02	129 ±15		
	1.00	172	5.03 ±0.05	300 ±6	102.0 ±1.0	99.4 ±2.0
Serum 6	0	0	4.16 ±0.01	160 ±2		
	1.00	172	5.22 ±0.08	325 ±16	106.0 ±1.5	95.9 ±4.9

Conflicts of interest

There are no conflicts to declare.

Acknowledgements

This work was supported by the National Natural Science Foundation of China (No. 21435001), the National First-class Discipline Program of Food Science and Technology (No. JUFSTR20180301), the Fundamental Research Funds for Central Universities (No. JUSRP51714B), and Open Funds of the State Key Laboratory of Electroanalytical Chemistry (SKLEAC201705).

References

1 U. P. Rohr, C. Binder, T. Dieterle, F. Giusti, C. G. Messina, E. Toerien, H. Moch and H. H. Schafer, *PloS one*, 2016, **11**, e0149856.
2 F. Lough, J. D. Perry, S. P. Stanforth and J. R. Dean, *TrAC, Trends Anal. Chem.*, 2017, **87**, 71-81.
3 D. Duffy, E. Mottez, S. Ainsworth, T. P. Buivan, A. Baudin, M. Vray, B. Reed, A. Fontanet, A. Rohel, V. Petrov-Sanchez, L. Abel, I. Theodorou, G. Miele, S. Pol and M. L. Albert, *PLoS One*, 2017, **12**, e0183084.
4 S. L. Cramer, A. Saha, J. Liu, S. Tadi, S. Tiziani, W. Yan, K. Triplett, C. Lamb, S. E. Alters, S. Rowlinson, Y. J. Zhang, M. J. Keating, P. Huang, J. DiGiovanni, G. Georgiou and E. Stone, *Nat. Med.*, 2017, **23**, 120-127.
5 S. Shankar and S. A. John, *Sens. and Actuators B: Chem.*, 2015, **221**, 1202-1208.
6 Z. Zheng, Q. Feng, J. Li and C. Wang, *Sens. and Actuators B: Chem.*, 2015, **221**, 1162-1169.
7 Y. Luo, L. Zhang, W. Liu, Y. Yu and Y. Tian, *Angew. Chem. Int. Ed. Engl.*, 2015, **54**, 14053-14056.
8 J. A. Paniagua, *World J Diabetes*, 2016, **7**, 483-514.
9 V. T. Samuel and G. I. Shulman, *Cell*, 2012, **148**, 852-871.
10 R. J. Perry, V. T. Samuel, K. F. Petersen and G. I. Shulman, *Nature*, 2014, **510**, 84-91.
11 B. Vandanmagsar, Y. H. Youm, A. Ravussin, J. E. Galgani, K. Stadler, R. L. Mynatt, E. Ravussin, J. M. Stephens and V. D. Dixit, *Nat. Med.*, 2011, **17**, 179-188.
12 M. Xu, X. Luo and J. J. Davis, *Biosens. Bioelectron.*, 2013, **39**, 21-25.
13 M. Wang, W. Wang, T. S. Kang, C. H. Leung and D. L. Ma, *Anal. Chem.*, 2016, **88**, 981-987.
14 M. S. Even, C. B. Sandusky, N. D. Barnard, J. Mistry and M. K. Sinha, *Clin. Biochem.*, 2007, **40**, 98-103.
15 K. V. Gobi, H. Iwasaka and N. Miura, *Biosens. Bioelectron.*, 2007, **22**, 1382-1389.
16 J. Hilderink, C. Otto, C. Slump, A. Lenferink, M. Engelse, C. van Blitterswijk, E. de Koning, M. Karperien and A. van Apeldoorn, *PLoS One*, 2013, **8**, e78148.
17 X. Jie, H. Yang, M. Wang, Y. Zhang, W. Wei and Z. Xia, *Angew. Chem. Int. Ed. Engl.*, 2017, **56**, 14596-14601.
18 W. Zhu, L. Xu, C. Zhu, B. Li, H. Xiao, H. Jiang and X. Zhou, *Electrochim. Acta*, 2016, **218**, 91-100.
19 Y. Jiang, M. Shi, Y. Liu, S. Wan, C. Cui, L. Zhang and W. Tan, *Angew. Chem. Int. Ed. Engl.*, 2017, **56**, 11916-11920.
20 J.-S. Lee, M. S. Han and C. A. Mirkin, *Angew. Chem.*, 2007, **119**, 4171-4174.
21 H. S. Jung, X. Chen, J. S. Kim and J. Yoon, *Chem. Soc. Rev.*, 2013, **42**, 6019-6031.
22 D. A. Giljohann, D. S. Seferos, P. C. Patel, J. E. Millstone, N. L. Rosi and C. A. Mirkin, *Nano Lett.*, 2007, **7**, 3818-3821.
23 Z. Li, Y. Zhang, X. Wu, L. Huang, D. Li, W. Fan and G. Han, *J. Am. Chem. Soc.*, 2015, **137**, 5304-5307.
24 Y.-J. Li, C.-X. Yang and X.-P. Yan, *Anal. Chem.*, 2018, **90**, 4188-4195.
25 M. P. Bui, S. Ahmed and A. Abbas, *Nano Lett.*, 2015, **15**, 6239-6246.
26 Q. Xiao, F. Shang, X. Xu, Q. Li, C. Lu and J.-M. Lin, *Biosens. Bioelectron.*, 2011, **30**, 211-215.

View Article Online
DOI: 10.1039/C8NR04414G

Graphic Abstract

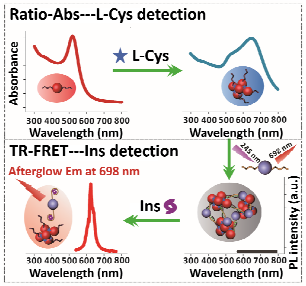

Functionalized gold and persistent luminescence nanoparticles based ratiometric absorption and TR-FRET nanoplatform shows new perspectives for sequential detection of multiple target in IVD, food safety inspection and environment monitoring.